

Revised on 2014 May 12 07:30PST

Physical Properties of Asteroids in Comet-like Orbits in Infrared Asteroid Survey Catalogs

Yoonyoung KIM, Masateru ISHIGURO¹

*Department of Physics and Astronomy, Seoul National University, Gwanak, Seoul 151-742, South
Korea*

and

Fumihiko USUI

*Department of Astronomy, Graduate School of Science, University of Tokyo,
7-3-1 Hongo, Bunkyo-ku, Tokyo 113-0033, Japan*

ABSTRACT

We investigated the population of asteroids in comet-like orbits using available asteroid size and albedo catalogs of data taken with the *Infrared Astronomical Satellite*, *AKARI*, and the *Wide-field Infrared Survey Explorer* on the basis of their orbital properties (i.e., the Tisserand parameter with respect to Jupiter, T_J , and the aphelion distance, Q). We found that (i) there are 123 asteroids in comet-like orbits by our criteria (i.e., $Q < 4.5$ AU and $T_J < 3$), (ii) 80% of them have low albedo, $p_v < 0.1$, consistent with comet nuclei, (iii) low-albedo objects among them have a size distribution shallower than that of active comet nuclei, that is, the power index of the cumulative size distribution of around 1.1, (iv) unexpectedly, a considerable number (i.e., 25 by our criteria) of asteroids in comet-like orbits have high albedo, $p_v > 0.1$. We noticed that such high-albedo objects mostly consist of small ($D < 3$ km) bodies distributed in near-Earth space (with perihelion distance of $q < 1.3$ AU). We suggest that such high-albedo, small objects were susceptible to the Yarkovsky effect and drifted into comet-like orbits via chaotic resonances with planets.

Subject headings: comets: general – comets: minor planets, asteroids — general

¹Visiting Scientist, Department of Earth, Planetary and Space Sciences, University of California at Los Angeles, 595 Charles Young Drive East, Los Angeles, CA 90095-1567, USA

1. Introduction

Comets, which consist of volatiles and dark (of typical geometric albedo $p_v = 0.02\text{--}0.06$; Campins & Fernández 2000; Lamy et al. 2004), reddish refractory, lose their volatiles near their surfaces after many re-turning orbits. Simultaneously, their surfaces are covered with an inert dust mantle that prevents sublimation of subsurface ice (Priolnik & Bar-Nun 1988; Rickman et al. 1990). Eventually, their appearances would be indistinguishable from asteroids through astronomical observations. It has been speculated that there could be dormant or extinct comets in the list of known asteroids. Because the physical lifetime of short-period comets in the inner Solar System ($\approx 1 \times 10^4$ years) is 10–1000 times longer than that of the devolatilization timescale of ices (Levison & Duncan 1997), it is not surprising that there would be hidden comets in the list of asteroids (Weissman et al. 2002; Jewitt 2004).

Identification of such dormant comets from telescopic observations is not simple because comet nuclei have a wide range of optical properties (i.e., albedos and reflectance spectra) that overlap those of some classes of asteroids. Meanwhile, the Tisserand parameter, T_J , derived from the Jacobi integral of the circular, restricted three-body problem of the Sun, Jupiter and an interplanetary body, provides a useful criterion for distinguishing comets from asteroids. It is defined by

$$T_J = \frac{a_J}{a} + 2 \left[(1 - e^2) \frac{a}{a_J} \right]^{1/2} \cos i, \quad (1)$$

where a_J ($= 5.2$ AU) is the semimajor axes of Jupiter, and a , e , and i are the semimajor axis, eccentricity, and inclination, respectively, of an interplanetary body such as a comet or asteroid. Comets usually have $T_J < 3$, whereas most asteroids have $T_J > 3$ (Levison & Duncan 1997).

An early survey of dormant comets was performed by Fernández et al. (2001, 2005). They conducted optical and infrared observations from ground to derive the albedo of asteroids in cometary orbits and found a clear correlation between the Tisserand parameter and albedo, suggesting that T_J is a good indicator to discriminate between asteroids and comets. A follow-up survey was performed by Licandro et al. (2008), using visible ($0.55\text{--}0.90 \mu\text{m}$) and near-infrared ($0.8\text{--}2.3 \mu\text{m}$) spectrographs. They determined the spectral taxonomic types of 24 asteroids in comet-like orbits and found that all observed objects with $T_J < 2.9$ have neutral or reddish spectra compatible with comet nuclei. In addition, DeMeo & Binzel (2008) acquired spectra of 20 near-Earth asteroids (defined by those having a perihelion distance $q < 1.3$ AU) in comet-like orbits. They estimated that $\sim 8\%$ of the observed near-Earth objects have surface spectral types consistent with comets.

Data taken with infrared space telescopes open up a further possibility to study dormant comets. At present, three infrared asteroid catalogs of data taken with infrared space surveyors are available, providing information about sizes and albedos that are useful in diagnosing the physical properties of dormant comets as well as asteroids. The principal aim of this study is to investigate the population of asteroids in comet-like orbits with these infrared catalogs, following the research of Fernández et al. (2001, 2005). In this paper, we adopt the term “asteroid in comet-like orbit” (ACO) as one having $T_J < 3.0$ and an aphelion distance $Q > 4.5$ AU. The term has

been occasionally used in some papers (Fernández et al. 2001, 2005; Licandro et al. 2006, 2008). Moreover, we introduce the term “potential dormant comet” (PDC) as one having low albedo ($p_v < 0.1$) among ACOs. The second term is a paronomasia associating the spectra of potential dormant comets with similar spectra of P-type, D-type, or C-type asteroids (Licandro et al. 2008; DeMeo & Binzel 2008). In Section 2, we describe the data sets and our extraction method for ACOs. In Section 3, we show our results on the physical properties of ACOs and PDCs. Finally, we discuss our findings and compare them with previous research in Section 4.

2. Applied Data and Methodology

2.1. Infrared Asteroid Catalogs

We used infrared asteroid databases compiled from three infrared all-sky surveyors, the *Infrared Astronomical Satellite* (*IRAS*; Neugebauer et al. 1984), *AKARI* (Murakami et al. 2007), and the *Wide-field Infrared Survey Explorer* (*WISE*; Wright et al. 2010). Detailed descriptions of the asteroid catalogs compiled from these surveyors can be found in Tedesco et al. (2002), Usui et al. (2011), and Mainzer et al. (2011), respectively, and their series of papers. These catalog data are available online.^{1 2}

Usui et al. (2014) compared these three infrared asteroidal catalogs with valid sizes and albedos and merged them into single catalog (I–A–W). They archived 138,285 asteroids with sizes and albedos, detected with either *IRAS*, *AKARI*, or *WISE* in I–A–W. A number of asteroids were detected by two or three satellites: 1993 asteroids by three satellites, 2812 asteroids by *AKARI* and *WISE*, and 312 asteroids by *IRAS* and *WISE*. In such cases, Usui et al. (2014) selected data from *AKARI* as the highest priority, *WISE* as the second, and *IRAS* as the third priority, although there are no remarkable differences in sizes and albedos among these catalogs. *AKARI* data were given highest priority because its data have less uncertainty than *WISE* in sizes and albedos for the largest asteroids. We applied the I–A–W catalog for the analysis of ACOs.

2.2. Data Processing

We summarize the extraction process in Figure 1. The details are as follows.

1. There are 138,285 asteroids whose albedos and sizes are given in the I–A–W catalog. We obtained the orbital elements and spectral types of asteroids in the infrared catalogs. We added

¹<http://sbn.psi.edu/pds/resource/imps.html>

²<http://darts.jaxa.jp/ir/AKARI/catalogue/AcuA.html>

the orbital elements of all 138,285 asteroids from the Lowell Observatory³ and the JPL Small-Body Database Browser.⁴ In addition, we referred to spectral taxonomic types of asteroids, if such information was available in Tholen (1984), Bus & Binzel (2002), Lazzaro et al. (2004), DeMeo & Binzel (2008), Licandro et al. (2008), and Carvano et al. (2010). After appending this ancillary information, we obtained an infrared asteroid catalog of size and albedo, together with spectral taxonomic types and orbital elements (see the top in Figure 1).

2. Second, we examined dynamical groups of asteroids according to their orbital elements. We followed the definition used in Zellner et al. (1985), where they defined dynamical groups of asteroids based on their osculating orbital elements. After classification of dynamical groups, we excluded asteroids in three dynamical groups – Jupiter Trojans ($5.05 \leq a \leq 5.35$ AU), Hildas ($3.7 < a \leq 4.2$ AU, $e \leq 0.3$, and $i \leq 20^\circ$), and Cybeles ($3.27 < a \leq 3.70$ AU, $e \leq 0.3$, and $i \leq 25^\circ$) – for extracting ACOs and PDCs, since these asteroids could be native objects trapped in these regions soon after the formation of the Solar System and are unlikely to be dormant comets recently captured in the current Solar System (Marzari & Scholl 1998; Kortenkamp et al. 2001; Levison et al. 2008; Morbidelli et al. 2005).
3. We calculated the Tisserand parameter, T_J . In general, a criterion of $T_J < 3$ has been applied for objects in comet-like orbits whereas $T_J > 3$ has been applied for objects in asteroidal orbits, although there are some exceptions for comets. Encke-type comets are visible active comets that have the Tisserand parameter $T_J > 3$. As of March 2014, there are only 39 comets having $T_J > 3$ among >600 short-period comets. Main-belt comets have orbits indistinguishable from main-belt asteroids ($T_J > 3$) but show comet-like activities owing to sublimation of ice, impacts, and so on (Jewitt 2012; Hsieh & Jewitt 2006). We excluded objects having $T_J \geq 3$, and we do not consider objects classified as Encke-type comets and main-belt comets because of the difficulty in discriminating them from the majority of asteroids.
4. Orbital uncertainty should be considered to extract ACOs from the catalog. We noticed that there is a large discrepancy in the orbital elements of some asteroids between Lowell Observatory and the JPL Small-Body Database Browser. In particular, the *WISE* mission discovered a number of new asteroids. Some of them are newly discovered asteroids whose orbital elements are not determined well because of inadequate orbital arcs and/or number of observations. Since the Tisserand parameters calculated with poorly determined orbital elements could lead to erroneous results, we computed the error of the Tisserand parameter, δT_J , and eliminated them from the list of ACOs unless the error was enough to distinguish ACOs from the majority of asteroids. We thus calculated δT_J with the following equation:

$$\delta T_J = \frac{\partial T_J}{\partial a} \delta a + \frac{\partial T_J}{\partial e} \delta e + \frac{\partial T_J}{\partial i} \delta i, \quad (2)$$

³<ftp://ftp.lowell.edu/pub/elgb/astorb.dat>

⁴<http://ssd.jpl.nasa.gov/>

where δa , δe , and δi are uncertainties of semimajor axis, eccentricity, and inclination, respectively, given by the JPL Small-Body Database Browser. We set the threshold for the elimination of δT_J to be >0.1 . We excluded 349 ACO candidates with $T_J < 3$ because of the large uncertainty in δT_J .

5. In addition, we adopted a criterion for the aphelion of $Q > 4.5$ AU following Fernández et al. (2002). This is an effective condition to exclude some main-belt asteroids (e.g., asteroids with high-inclined orbits). For comparison, we examined the orbital elements of active comets in the JPL Small-Body Database Search Engine⁵ and found that all except 12 Encke-type comets and 10 main-belt comets have $Q > 4.5$ AU (as of March 2014). Because we do not consider Encke-type comets and main-belt comets, we set the criterion $Q > 4.5$ AU.
6. Although we excluded the Hilda group above, 41 objects that marginally do not fall into the category of the Hilda group still remained. Their osculating semimajor axes fall into the Hilda group (i.e., $3.7 < a < 4.2$ AU) but they have eccentricity and/or inclination slightly larger than the Hilda asteroids. As we discuss later, we excluded 38 objects among them and regarded only 3 objects as ACOs.

⁵<http://ssd.jpl.nasa.gov/sbdb-query.cgi>

3. Results

In this section, we examine the albedos of ACOs extracted based on the criteria in Section 2.2 and define the PDCs that have comets-like orbits (i.e., $T_J < 3.0$ and $Q > 4.5$ AU) and comet-like albedos ($p_v < 0.1$). Then, we study the physical characteristics of PDCs and the other ACOs.

3.1. Albedo Properties of ACOs and Extraction of PDCs

Figure 2(a) shows the histogram of geometric albedos of ACOs. For comparison, we provide the albedo histogram of ACOs with a criterion for the Tisserand parameter, i.e., $T_J < 2.6$, suggested by Fernández et al. (2005) because it provides a more assured condition for extracting comet-like objects. There is, however, no big differences between the two criterion of T_J in our sample of ACOs. Since the appearance of histogram may depend on the choice of the bin width (Δp_v), we changed it from $\Delta p_v = 0.005$ to 0.015 but could not find any significant differences in the appearances. The histogram shows a prominent peak with a mode around 0.04–0.05. Our sample of ACOs includes some objects with high albedos regardless of the severe T_J criterion. Figure 2(b) compares our sample of ACOs with that of active comets based on the data in Lamy et al. (2004), together with a few samples from Usui et al. (2011) and Bauer et al. (2013). Comets have a mean albedo of 0.046 with a standard deviation of 0.020 if we fit a Gaussian function. Because no comets have albedo > 0.1 , we placed the upper limit of comet-like albedo at 0.1. Our upper bound of comet-like albedo (i.e., $p_v = 0.1$) is slightly higher than that in Fernández et al. (2001, 2005), where they adopted the comet-like albedo of $p_v < 0.075$. The difference seems to be trivial, but we used the criterion of $p_v = 0.1$ because a few comet nuclei with higher albedo ($p_v > 0.075$) were recognized ($p_v = 0.096$ for 212P and $p_v = 0.101$ for C/2011 KP36) by Fernández et al. (2005) and Bauer et al. (2013).

The average albedo of PDCs is $p_v = 0.049 \pm 0.020$, which is similar to those of the active comet nuclei mentioned above ($p_v = 0.046 \pm 0.020$). A peak in the PDC distribution appears near 0.04–0.05, which is consistent with the peak in the comet albedo distribution. These similarities suggest that we have extracted dormant comets from the asteroid catalogs in an appropriate manner.

3.2. Size Distribution of PDCs

The size distribution of an ensemble of minor bodies gives us information helpful for explaining their source region and evolutionary history. The cumulative size distribution has been applied in previous research. It is approximated by the mathematical form

$$N_S(> D) \propto D^{-q_S}, \quad (3)$$

where $N_S(> D)$ is the cumulative number of bodies larger than diameter D , and q_S denotes the power index of the cumulative size distribution.

We examined the cumulative size distribution of PDCs in terms of two different origins: Jupiter-family comets (JFCs), considered to originate from the scattered disk of the Solar System (Levison & Duncan 1997), and nearly-isotropic comets (NICs), originating from the Oort cloud (Weissman et al. 2002). In some of the literature, NICs are further subdivided into long-period comets with orbital period $P > 200$ years and Halley-type comets with $P < 200$ years. We separated our samples into two groups, one having $2 < T_J < 3$ (PDCs in JFC-like orbits) and another having $T_J < 2$ (PDCs in NIC-like orbits).

Figure 3 shows the cumulative size distributions of PDCs in JFC-like orbits (a) and PDCs in NIC-like orbits (b). We incorporate 11 PDCs from Fernández et al. (2001, 2005) in our list, so that the total number of PDCs increased from 83 to 94. These size distributions are compared with those of active comets. In Figure 3, we applied the sizes of active JFCs in Fernández et al. (2013) and active NICs in Lamy et al. (2004). We found that PDCs have a shallower size distribution than active comets, although the number of samples for NICs (only 17 PDCs in the NIC class) may not be significant for a statistical discussion. Careful comparison between PDCs in JFC-like orbits and active comets makes us aware that the size distributions show good agreement in the small-size range $2 < D < 4$ km, that is, $q_S = 1.0$ for PDCs and $q_S = 1.1$ for JFC nucleus; however, they show a significant discrepancy in slope in the big-size range (4–10 km in diameter), that is, $q_S = 1.11 \pm 0.04$ for PDCs and $q_S = 1.9$ for active JFCs (Fernández et al. 2013).

3.3. Spectral Types

We have eight ACOs whose spectral taxonomic types are known. There are one C-type object (7604 Kridsadaporn), four D-type objects (944 Hidalgo, 3552 Don Quixote, 6144 Kondojiro, and 20898 Fountainhills), and three X- or P-type objects (3688 Navajo, P/2006 HR30, and 2001 XP1). The X-type (Tholen 1984) has subcategories depending on the albedo measurements: E- and M-types for high albedos and medium albedos and P-type for the low albedos equivalent to comets (i.e., $p_v < 0.1$). We classify two X-type ACOs as of P-type, according to their low albedos. All eight objects have significantly low albedo ($p_v < 0.06$). We examined the spectral slopes S' of these eight objects, which express the percentage change in the reflectance per 1000 Å of wavelength difference (Jewitt 2002). We computed the slope of four objects (7604 Kridsadaporn, 944 Hidalgo, 3552 Don Quixote and 2001 XP1). Together with the S' values in DeMeo & Binzel (2008) and Licandro et al. (2008), we obtained $S' = 5.7 \pm 4.8$, which is consistent with the slopes of dormant comet candidates ($7.2 \pm 2.0\%$) and comet nuclei ($8.3 \pm 2.8\%$) (Jewitt 2002). Therefore, we conclude that these eight objects are most likely PDCs. In fact, P/2006 HR30 and 3552 Don Quixote showed comet-like activities after their discovery as asteroids (Hicks & Bauer 2007; Mommert et al. 2014).

3.4. High-Albedo ACOs

We identified a peculiar population of ACOs that have high albedos unlike comet nuclei; this is an unexpected population. Because we excluded objects with $\delta T_J > 0.1$, they are not caused by inaccuracy in their orbital elements. The total divergence among I–A–W is 10% in diameter and 22% in albedo at the 1σ level (Usui et al. 2014), which is small enough to justify the existence of ACOs with high albedo. Therefore, it is likely that there are high-albedo asteroids in comet-like orbits.

To understand the unexpected population, we studied the physical characteristics of these high-albedo ACOs. Figure 4 shows a plot of diameter against perihelion distance for all ACOs (a) and ACOs with $T_J < 2.6$ (b). Note that the paucity of small ACOs beyond $q \sim 2$ AU is an observational bias. We found a pronounced tendency for high-albedo ACOs to concentrate in near-Earth space (i.e., $q < 1.3$ AU). In addition, they consist of small asteroids (< 3 km). In Figure 4, there are four high-albedo ACOs at $q > 1.3$ AU. Among them, three objects have albedo of $p_v \sim 0.1$, that is, 2009 QK35 ($p_v = 0.10 \pm 0.03$), 2010 MB86 ($p_v = 0.11 \pm 0.03$), and 2010 MK43 ($p_v = 0.10 \pm 0.03$), and one object, 2010 RM64 ($p_v = 0.16 \pm 0.05$), marginally has high albedo. Thus, nearly all high-albedo ACOs consist of small asteroids at $q < 1.3$ AU. This trend cannot be explained by the observational bias. Because the result is obtained based on the mid-infrared data, which, unlike optical observations, are less sensitive to albedo values, it provides reliable sets of asteroid albedo information. If there are big ACOs with high albedo beyond $q = 1.3$ AU, they would be detected easily. Although further dynamical study is essential to evaluate the population quantitatively, we propose that such ACOs with high albedos were injected from the domain of $T_J > 3$ via the Yarkovsky effect, because small objects with higher surface temperature are susceptible to the thermal drag force and gradually change their orbital elements to be observed as ACOs in our list.

4. Discussion

4.1. Comparison with Previous Research

In this subsection, we compare our results with those from previous research on ACOs. Fernández et al. (2001, 2005) found that nearly all objects in their sample with $T_J < 2.6$ have comet-like albedos ($p_v < 0.075$), implying that objects with $T_J < 2.6$ are most likely dormant comets. They also found that the transition region $2.6 < T_J < 3$ comprises a mixture of high-albedo and low-albedo objects, suggesting that the region is populated by a variety of sources. A similar argument was made by Licandro et al. (2006, 2008), who insisted that a criterion of $T_J < 2.7$ provides the most reliable sets of PDCs based on their spectral survey of ACOs. Following the work by Fernández et al. (2001, 2005), we made a plot of geometric albedo with respect to T_J (Figure 5). As suggested by Fernández et al. (2001, 2005), we confirm the similar trend that most objects with small T_J have low albedo. However, our results differ from those of Fernández et al. (2001, 2005) and Licandro et al. (2006, 2008) in that we find high-albedo objects in the region $T_J < 2.6$. Because Fernández et al. (2001, 2005) detected small objects (< 3 km), it is not surprising that they potentially detected ACOs with high albedo in the region of $T_J < 2.6$. It is not clear why they did not detect such ACOs with high albedo. A possible explanation of such high-albedo objects is the inadequate measurements of optical magnitudes in our samples. In fact, Fernández et al. (2001, 2005) measured both optical and infrared magnitudes simultaneously by themselves with ground-based telescopes, providing reliable albedo data, whereas our infrared survey data relied on absolute magnitudes in which there is an intrinsic difficulty in determining the absolute magnitudes and eventually the albedos (Harris & Harris 1997; Pravec et al. 2012).

To refute the uncertain factor related to optical magnitudes, we observed three objects: 2006 HY51 ($p_v = 0.157 \pm 0.071$, $T_J = 2.30$), 2006 CS ($p_v = 0.037 \pm 0.021$, $T_J = 2.44$), and 2010 NY1 ($p_v = 0.037 \pm 0.008$, $T_J = 2.66$). We made optical observation of these ACOs with the Faint Object Camera and Spectrograph (FOCAS; Kashikawa et al. 2002) attached to the 8.2-m Subaru Telescope atop Mauna Kea (Hawaii, USA) on June 5, 2013 (UT). Flux calibration was performed using SA 104-430, SA 110-361, and MARK A2 listed in Landolt (1992). The observed magnitudes were converted into absolute magnitudes by assuming a phase slope of $0.035 \text{ mag deg}^{-1}$ (Lamy et al. 2004). We obtained absolute V magnitudes of 17.18 ± 0.30 (2006 HY51), 16.76 ± 0.09 (2006 CS), and 17.07 ± 0.21 (2010 NY1), respectively. These are consistent with the magnitude used by Mainzer et al. (2011, 2012), who employed 17.20, 16.60, and 16.70, respectively. Therefore, it is unlikely that optical magnitudes led to poor albedo values, at least for these three ACOs.

With Subaru, we derived the color of one object, 2006 CS ($p_v = 0.037 \pm 0.021$), as $(V - R) = 0.341 \pm 0.126$ and $(B - V) = 0.599 \pm 0.149$. These indices are less red than the average comet nucleus but in the possible range of PDCs. We could not derive the color of the other two objects because of the faintness at the time of our observation. Instead, we found the spectrum of 2006 HY51

archived in SMASS.⁶ Although 2006 HY51’s taxonomic type is not identified, it exhibits several key features typical of siliceous (e.g., S-type) asteroids having a red continuum at 1–1.5 μm and shallow absorption around 2 μm , probably associated with the presence of pyroxene (Gaffey et al. 1993). Together with the moderately high albedo ($p_v = 0.157 \pm 0.071$ as determined from *WISE*) and the spectrum, we may conclude that 2006 HY51 is not a dormant comet nucleus but is a high-albedo ACO.

4.2. Asteroids in Comet-like Orbits near the Hilda Region

In the I–A–W catalog, we found that there are a considerable number of objects having $T_J < 3$ but not categorized as ACOs by our criteria (see Section 2.2), that is, 1764 in Jupiter Trojans, 432 in the Hilda region, and 104 in the Cybele region. Theoretical studies suggested that the Trojans were captured during the early stages of Jupiter’s growth (Marzari & Scholl 1998) or via the effects of nebular gas (Kortenkamp et al. 2001). More recently, it has been suggested that they were captured during planetary migration, which occurred about 500–600 million years after the Solar System’s formation (Levison et al. 2008; Morbidelli et al. 2005). In either case, it may be true that Jupiter Trojans were objects trapped in the early stage of the Solar System’s formation and not dormant comets captured recently. The Hilda asteroids are in another region populated by interplanetary bodies in the 3:2 inner mean motion resonance with Jupiter. Because of their stable orbits, the Hilda asteroids are also considered to be objects formed in the early stage of the Solar System, although there are about 10–20 comets that have been captured temporarily in the Hilda region (Ohtsuka et al. 2008; Toth 2006). The Hilda asteroids are defined as objects that have osculating orbital elements $3.7 < a \leq 4.2$ AU, $e \leq 0.3$, and $i \leq 20^\circ$. As we described in Section 2.2, there are a considerable number of objects (42) with $T_J < 3.0$ that marginally fall off the conditions of the Hilda group. Figure 6 shows the histograms of semimajor axis and eccentricity of ACOs, including objects close to the Hilda asteroids. There is an unnatural prominent peak near the edge of the Hilda region ($a \sim 4.0$ AU, $e \sim 0.3$). We investigated the dynamical stability of 42 ACOs using the dynamical integration code Mercury 6 (Chambers 1999). We thus integrated their orbits forward for 100,000 years (longer than the physical time scale of short-period comets). We found that all but three objects have stable orbits over the timescale of 100,000 years. Although there are uncertainties in the dynamical simulation such as the value of the Yarkovsky force and the rocket force (for active comets), we conservatively consider that these three objects (2000 SU236, 2008 UM7, and 2009 SC298) are ACOs and PDCs.

Let us consider how the Yarkovsky effect moves an asteroid into a comet-like orbit. As shown in Figure 7(a), high-albedo ACOs concentrate in a range of $2 < a < 3.5$ AU, similar to main-belt asteroids and JFCs. The Tisserand parameter is a function of a , e , and i , while the Yarkovsky effect changes a . Due to the similarity in a between high-albedo ACOs and main-belt asteroids,

⁶<http://smass.mit.edu/smass.html>

we would conjecture that subsequent dynamical effects may change e and i . As widely known as a standard model for orbital evolution of near-Earth asteroids, the Yarkovsky effect could move small main-belt asteroids’ orbits until they are close to resonances with planets, and subsequently, these resonances can push them in terrestrial planet crossing orbits (see e.g. Morbidelli et al. 2002). Numerical simulations demonstrated that chaotic resonances cause a significant increase in their e and i of test particles in the resonance regions (Gladman et al. 1997). Bottke et al. (2002) suggested that some objects on $T_J < 3$ (or even $T_J < 2$) can result from chaotic resonances. We reviewed the semimajor axes of ACOs in our list. Figure 8 shows a - e plot of ACOs together with major resonances. Although there are a couple of ACOs close to resonances, their semimajor axes are not related to these major resonances. Therefore, it may be reasonable to think that encounters with terrestrial planets as well as chaotic resonances with massive planets can drift main-belt asteroids into comet-like orbits.

4.3. Discussion of the Size Distribution of PDCs

Over the past decade, a number of attempts have been made to derive the size distributions of active comets (Lamy et al. 2004; Meech et al. 2004; Snodgrass et al. 2011; Fernández et al. 2013) and dormant comets (Alvarez-Candal & Licandro 2006; Whitman et al. 2006). These research results exhibit a wide range of the power index of the cumulative size distribution, that is, $q_S = 1.5$ – 2.7 for active comets and $q_S = 1.5$ – 2.6 for dormant comets. Most of this research (except that of Fernández et al. (2013)) was conducted by using optical magnitudes of these objects. Note that the observed quantity (i.e., magnitude) is proportional to the product of the albedo and the square of the size, and in these research studies albedo values were assumed. In addition, the phase-angle dependence of magnitudes is also presumed in these studies. Since the data taken in the mid-infrared wavelength provide the size of the objects without any albedo assumption, they yield a reliable data set of the size distribution of active comets and dormant comets.

We therefore compare the power exponents of active JFCs, $q_S \sim 1.9$ (Fernández et al. 2013), with that of PDCs, $q_S = 1.11 \pm 0.04$ (this work). Because the difference is significantly larger than those of the errors of measurements, this indicates that a physical mechanism is responsible for creating the difference in the course of cometary evolution. The moderate slope of the size distribution for PDCs ($q_S = 1.11 \pm 0.04$) implies that big objects are more abundant in the list of dormant objects. The splitting of comets, a phenomena that has been occasionally observed, can be a possible mechanism leading to the change in the power exponents. A good example event was observed at 73P/Schwassmann-Wachmann 3, in which the comet nucleus was ground into 10–100 m bodies. The power exponents of the cumulative size distribution of the fragments was ~ -2.3 (Ishiguro et al. 2009; Fuse et al. 2007). If the splitting is a principal mechanism in determining the size distribution of comet nuclei, the size distribution of PDCs might be steeper than the value we derived for PDCs. Another explanation is that big comet nuclei may develop inert surface dust layers more effectively than small ones because dust particles with small ejection velocity cannot

escape from the big nuclei against the gravitational force and eventually form surface dust layers that insulates subsurface ice against solar heating and/or choke off ice sublimation. A similar argument was made by Tancredi et al. (2006), who mentioned the possible choking mechanism on the large comet nuclei of 49P/Arend–Regaux and 28P/Neujmin 1.

We also should consider the observational bias. Big objects are favorably detected at distant locations. Figure 7(a) shows the diameter of ACOs as a function of the semimajor axis a . In the figure, it is clear that only big ACOs were detected beyond $a \sim 3.5$ AU, most likely because of the observation selection bias. We plotted the size distribution of PDCs within $a < 3.5$ AU to evaluate the effect. Figure 7(b) shows a comparison of the size distribution between all PDCs and PDCs within $a < 3.5$ AU. Although there is a large discrepancy in the largest size probably because of the insignificant number of samples, the slopes are consistent with one another in the size range of 2–4 km. In addition, we adopted a criterion to eliminate the observational bias in Alvarez-Candal & Licandro (2006), and obtained $q_S=1.27$. Although the power exponent is sensitive to the criteria we selected, we can safely say q_S is around 1.1 (neither <0.8 nor >1.3). Therefore, we may rule out the possibility of observational selection bias. In summary, rapid growth of a dust mantle on the big comet nuclei favors the obtained size exponent of PDCs.

5. Summary

In this paper, we address the question of the existence of dormant comets in the list of asteroids. Motivated by the recent developments of infrared asteroid catalogs (I–A–W) taken with three infrared surveyors (Usui et al. 2014), we identified ACOs with the criteria we contrived, i.e., $T_J < 3.0$ and $Q > 4.5$ AU. The major findings of our research are as follows:

1. There are 123 ACOs in the I–A–W catalog after rejection of objects with large orbital uncertainties.
2. The majority ($\sim 80\%$) of ACOs have comet-like albedo (i.e., $p_v < 0.1$).
3. Low-albedo ACOs (referred to as PDCs) have an albedo distribution similar to that of active comets, that is, $p_v = 0.049 \pm 0.020$. They have a shallower size distribution than that of active comets (i.e. $q_S \sim 1.1$).
4. Nearly all high-albedo ACOs consist of small bodies distributed in near-Earth orbit.

In particular, we stress again the significance of high-albedo ACOs. As we discussed through our ground-based observation with the Subaru Telescope, high-albedo ACOs, which may have composition similar to siliceous asteroids, definitively exist in the I–A–W database. Considering the very low T_J as well as the small size and perihelion distance, we would suggest that such high-albedo ACOs have been injected via nongravitational forces, most likely the Yarkovsky effect.

Acknowledgments

This work was supported by the National Research Foundation of Korea (NRF) funded by the South Korean government (MEST) (Grant No. 2012R1A4A1028713). This study is based on observations with *AKARI*, a JAXA project with the participation of ESA. This work also makes use of data products from the *Wide-field Infrared Survey Explorer*, which is a joint project of the University of California, Los Angeles, and the Jet Propulsion Laboratory/California Institute of Technology, funded by the National Aeronautics and Space Administration. Optical data were partially collected at the Subaru Telescope, which is operated by the National Astronomical Observatory of Japan. We thank T. Kasuga and R. Brasser for their valuable comments and T. Hattori for supporting observations at Subaru. We also thank anonymous referee for valuable comments. MI would like to express his gratitude to D. Jewitt for a support during his stay at UCLA. Part of the data utilized in this publication were obtained from SMASS, which were made available by the MIT-UH-IRTF Joint Campaign for NEO Spectral Reconnaissance.

REFERENCES

- Alvarez-Candal, A., & Licandro, J. 2006, *A&A*, 458, 1007
- Bauer, J. M., Grav, T., Blauvelt, E., et al. 2013, *ApJ*, 773, 22
- Bottke, W. F., Morbidelli, A., Jedicke, R., et al. 2002, *Icarus*, 156, 399
- Bus, S. J., & Binzel, R. P. 2002, *Icarus*, 158, 146
- Campins, H., & Fernández, Y. 2000, *Earth, Moon, Planets*, 89, 117
- Carvano, J. M., Hasselmann, P. H., Lazzaro, D., & Mothé-Diniz, T. 2010, *A&A*, 510, A43
- Chambers, J. E. 1999, *MNRAS*, 304, 793
- DeMeo, F., & Binzel, R. P. 2008, *Icarus*, 194, 436
- Fernández, Y. R., Kelley, M. S., Lamy, P. L., et al. 2013, *Icarus*, 226, 1138
- Fernández, J. A., Gallardo, T., & Brunini, A. 2002, *Icarus*, 159, 358
- Fernández, Y. R., Jewitt, D. C., & Sheppard, S. S. 2001, *ApJ*, 553, L197
- Fernández, Y. R., Jewitt, D. C., & Sheppard, S. S. 2005, *AJ*, 130, 308
- Fuse, T., Yamamoto, N., Kinoshita, D., Furusawa, H., & Watanabe, J.-I. 2007, *PASJ*, 59, 381
- Gaffey, M. J., Burbine, T. H., Piatek, J. L., et al. 1993, *Icarus*, 106, 573
- Gladman, B. J., Migliorini, F., Morbidelli, A., et al. 1997, *Science*, 277, 197
- Harris, A. W., & Harris, A. W. 1997, *Icarus*, 126, 450
- Hicks, M. D., & Bauer, J. M. 2007, *ApJ*, 662, L47
- Hsieh, H. H., & Jewitt, D. 2006, *Science*, 312, 561
- Ishiguro, M., Usui, F., Sarugaku, Y., & Ueno, M. 2009, *Icarus*, 203, 560
- Jewitt, D. 2012, *AJ*, 143, 66
- Jewitt, D. C. 2002, *AJ*, 123, 1039
- Jewitt, D. C. 2004, *Comets II*, 659
- Kashikawa, N., Aoki, K., Asai, R., et al. 2002, *PASJ*, 54, 819
- Kortenkamp, S. J., Wetherill, G. W., & Inaba, S. 2001, *Science*, 293, 1127
- Lamy, P. L., Toth, I., Fernandez, Y. R., & Weaver, H. A. 2004, *Comets II*, 223

- Landolt, A. U. 1992, *AJ*, 104, 1, 340
- Lazzaro, D., Angeli, C. A., Carvano, J. M., et al. 2004, *Icarus*, 172, 179
- Levison, H. F., & Duncan, M. J. 1997, *Icarus*, 127, 13
- Levison, H. F., Morbidelli, A., Van Laerhoven, C., Gomes, R., & Tsiganis, K. 2008, *Icarus*, 196, 258
- Licandro, J., Alvarez-Candal, A., de León, J., et al. 2008, *A&A*, 487, 1195
- Licandro, J., de León, J., Pinilla, N., & Serra-Ricart, M. 2006, *Adv Space Res*, 38, 1991
- Mainzer, A., Grav, T., Bauer, J., et al. 2011, *ApJ*, 743, 156
- Mainzer, A., Grav, T., Masiero, J., et al. 2012, *ApJ*, 760, L12
- Marzari, F., & Scholl, H. 1998, *A&A*, 339, 278
- Meech, K. J., Hainaut, O. R., & Marsden, B. G. 2004, *Icarus*, 170, 463
- Mommert, M., Hora, J. L., Harris, A. W., et al. 2014, *ApJ*, 781, 25
- Morbidelli, A., Bottke, W. F., Jr., Froeschlé, C., & Michel, P. 2002, *Asteroids III*, 409
- Morbidelli, A., Levison, H. F., Tsiganis, K., & Gomes, R. 2005, *Nature*, 435, 462
- Murakami, H., Baba, H., Barthel, P., et al. 2007, *PASJ*, 59, 369
- Neugebauer, G., Soifer, B. T., Miley, G., et al. 1984, *ApJ*, 278, L83
- Ohtsuka, K., Ito, T., Yoshikawa, M., Asher, D. J., & Arakida, H. 2008, *A&A*, 489, 1355
- Pravec, P., Harris, A. W., Kušnirák, P., Galád, A., & Hornoch, K. 2012, *Icarus*, 221, 365
- Prialnik, D., & Bar-Nun, A. 1988, *Icarus*, 74, 272
- Rickman, H., Fernandez, J. A., & Gustafson, B. A. S. 1990, *A&A*, 237, 524
- Snodgrass, C., Fitzsimmons, A., Lowry, S. C., & Weissman, P. 2011, *MNRAS*, 414, 458
- Tancredi, G., Fernández, J. A., Rickman, H., & Licandro, J. 2006, *Icarus*, 182, 527
- Tedesco, E. F., Noah P. V., Noah, M., & Price, S. D. 2002, *AJ*, 123, 1056
- Tholen, D. J. 1984, Ph.D. Thesis, University of Arizona, Tucson
- Toth, I. 2006, *A&A*, 448, 1191
- Usui, F., Kuroda, D., Müller, T. G., et al. 2011, *PASJ*, 63, 1117

- Usui, F., et al. 2014, PASJ, 66, 3 (in press)
- Weissman, P. R., Bottke, W. F., Jr., & Levison, H. F. 2002, Asteroids III, 669
- Whitman, K., Morbidelli, A., & Jedicke, R. 2006, Icarus, 183, 101
- Wright, E. L., Eisenhardt, P. R. M., Mainzer, A. K., et al. 2010, AJ, 140, 1868
- Zellner, B., Thirunagari, A., & Bender, D. 1985, Icarus, 62, 505

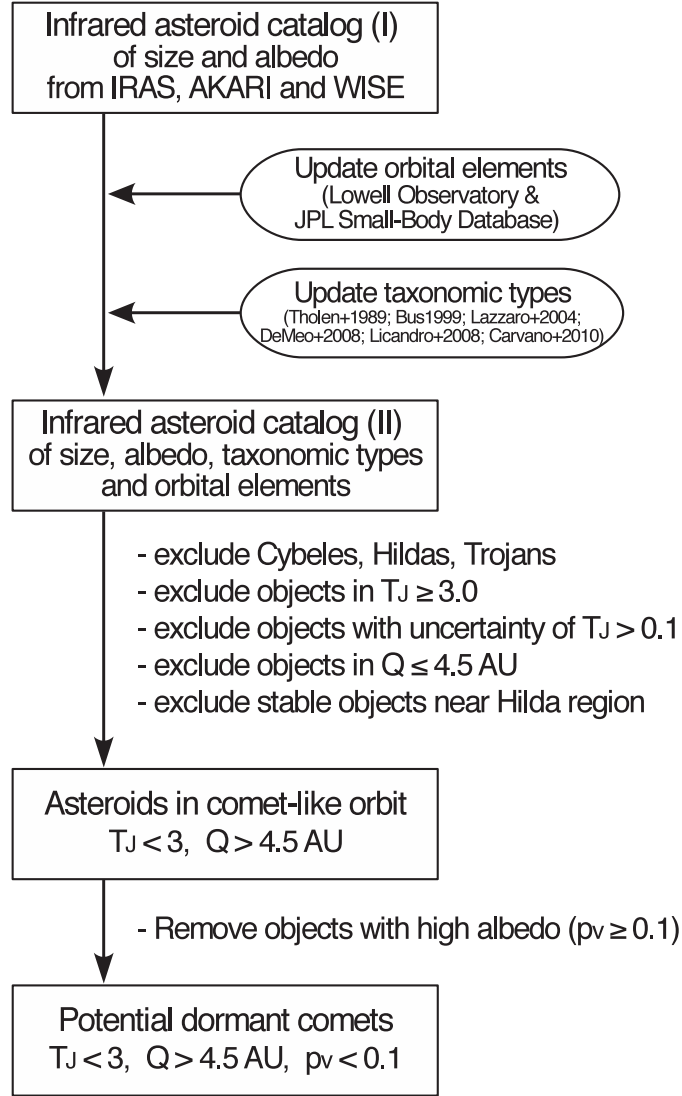


Fig. 1.— Schematic diagram of the extraction flow. See Section 2.2.

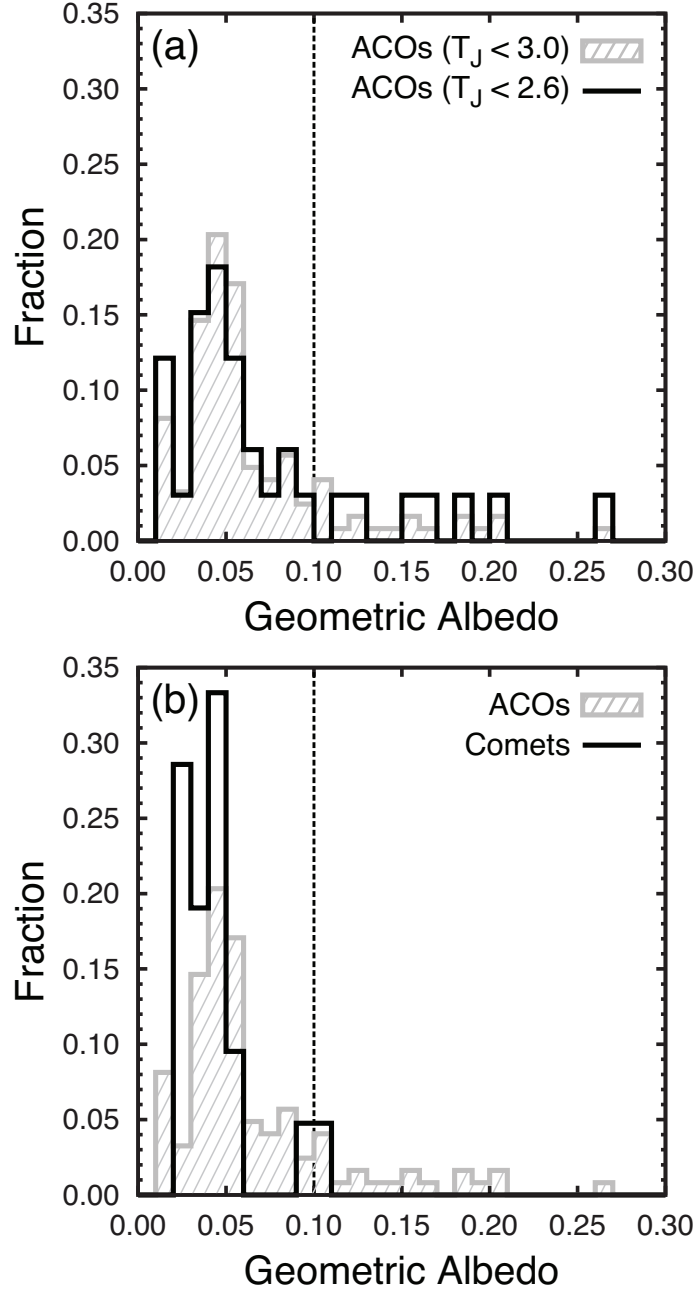


Fig. 2.— Histogram of albedos of asteroids in comet-like orbits (ACOs). (a) Albedo distributions of ACOs with different T_J criteria, that is, $T_J < 3$ and $T_J < 2.6$ following Fernández et al. (2005). (b) Albedo distribution of ACOs and active comets.

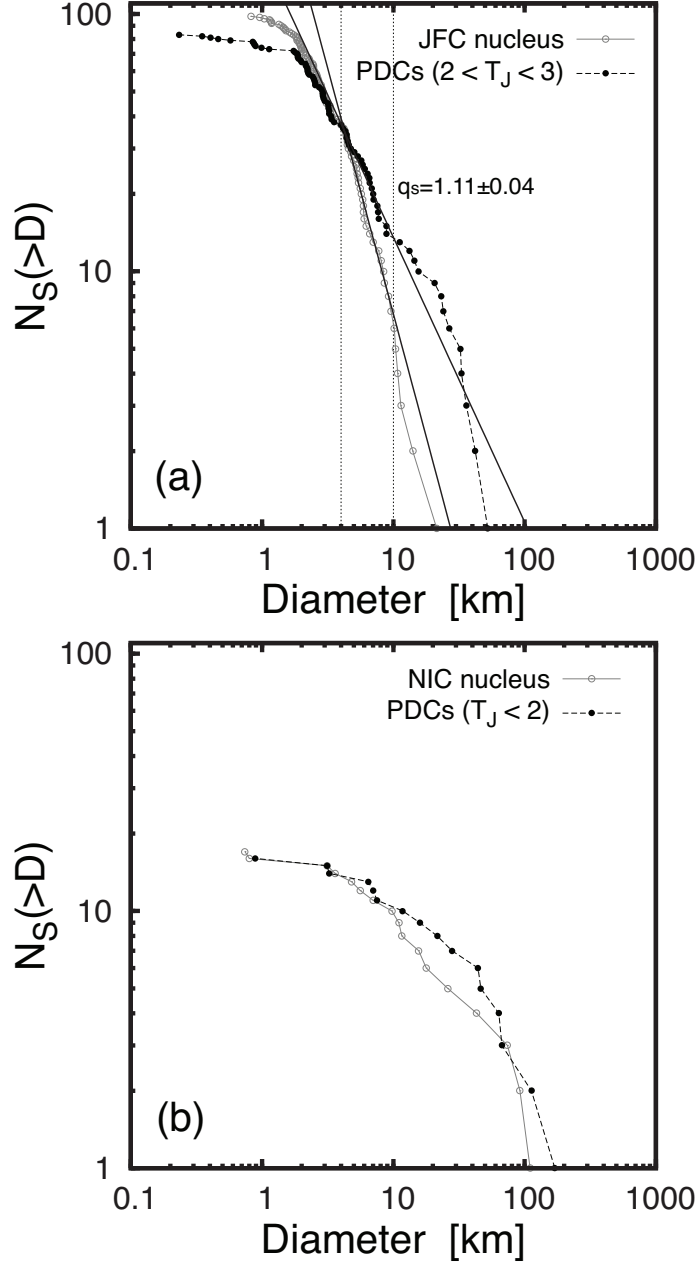


Fig. 3.— Cumulative size distribution of PDCs (filled circles) and ACOs (open circles). (a) Comparison between PDCs having $2 < T_J < 3$ and active JFCs. (b) Comparison between PDCs having $T_J < 2$ and active NICs.

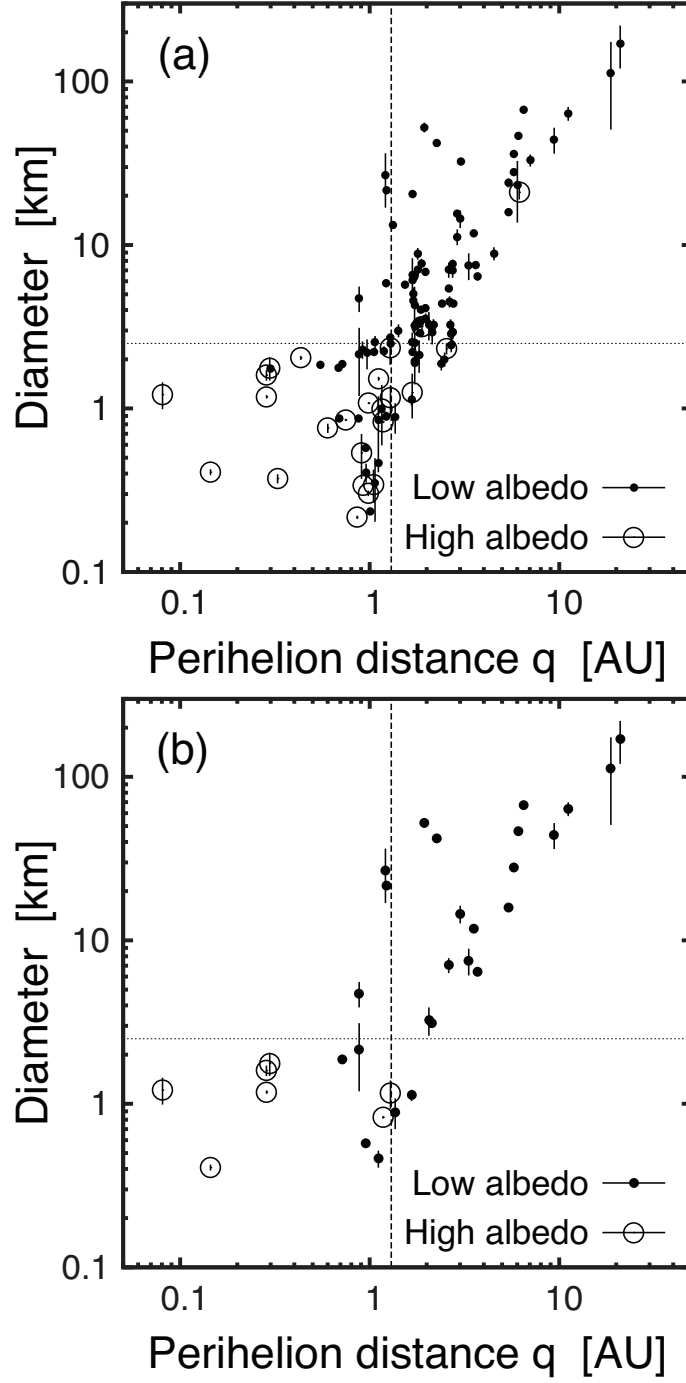


Fig. 4.— Plot of the perihelion distance q vs. the diameter of all ACOs (a) and ACOs with $T_J < 2.6$ (b). The open circles denote the high-albedo objects ($p_v \geq 0.1$); the filled circles denote the low-albedo objects ($p_v < 0.1$). We draw two lines for the perihelion distance at 1.3 AU (vertical line) and the diameter at 2.5 km (horizontal line) to discriminate small near-Earth objects (lower left).

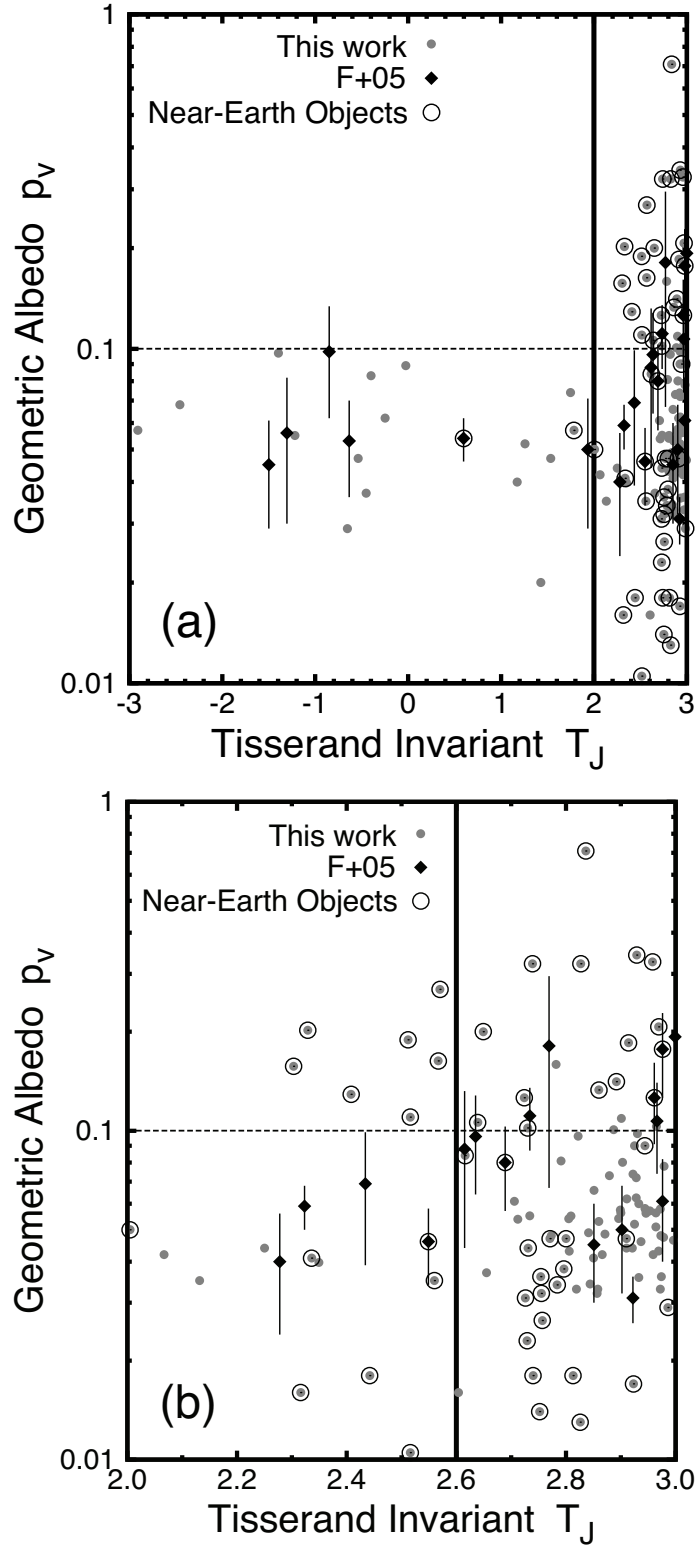


Fig. 5.— Plots of the Tisserand parameter T_J vs. geometric albedos in the range of $-3 < T_J < 3$ (top) and $2 < T_J < 3$ (bottom). For comparison, we show the result in Fernández et al. (2005), which is indicated by ‘F+05’ in the figures. Data points of near-Earth objects are enclosed by circles. The horizontal line corresponds to $p_v = 0.1$.

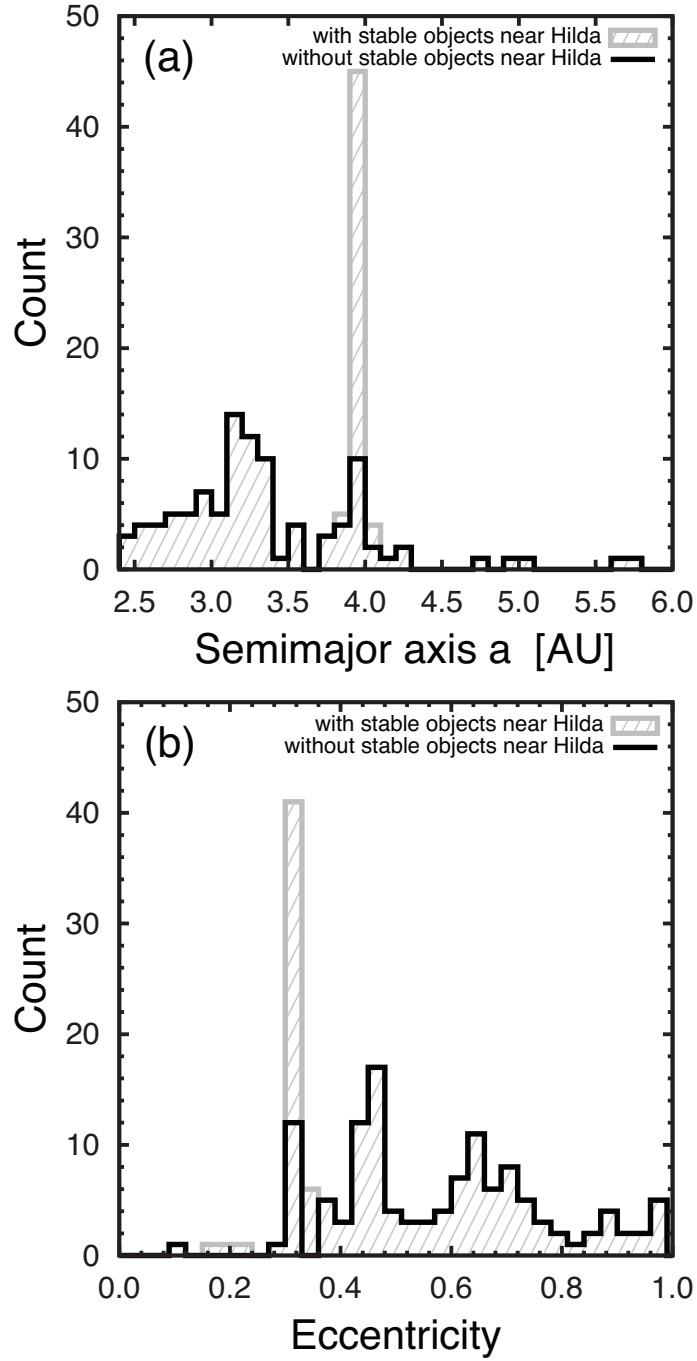


Fig. 6.— Histograms of semimajor axis and eccentricity of ACOs including the Hilda-like objects. There is a unnatural prominent peak near the Hilda regions (see Section 4.2).

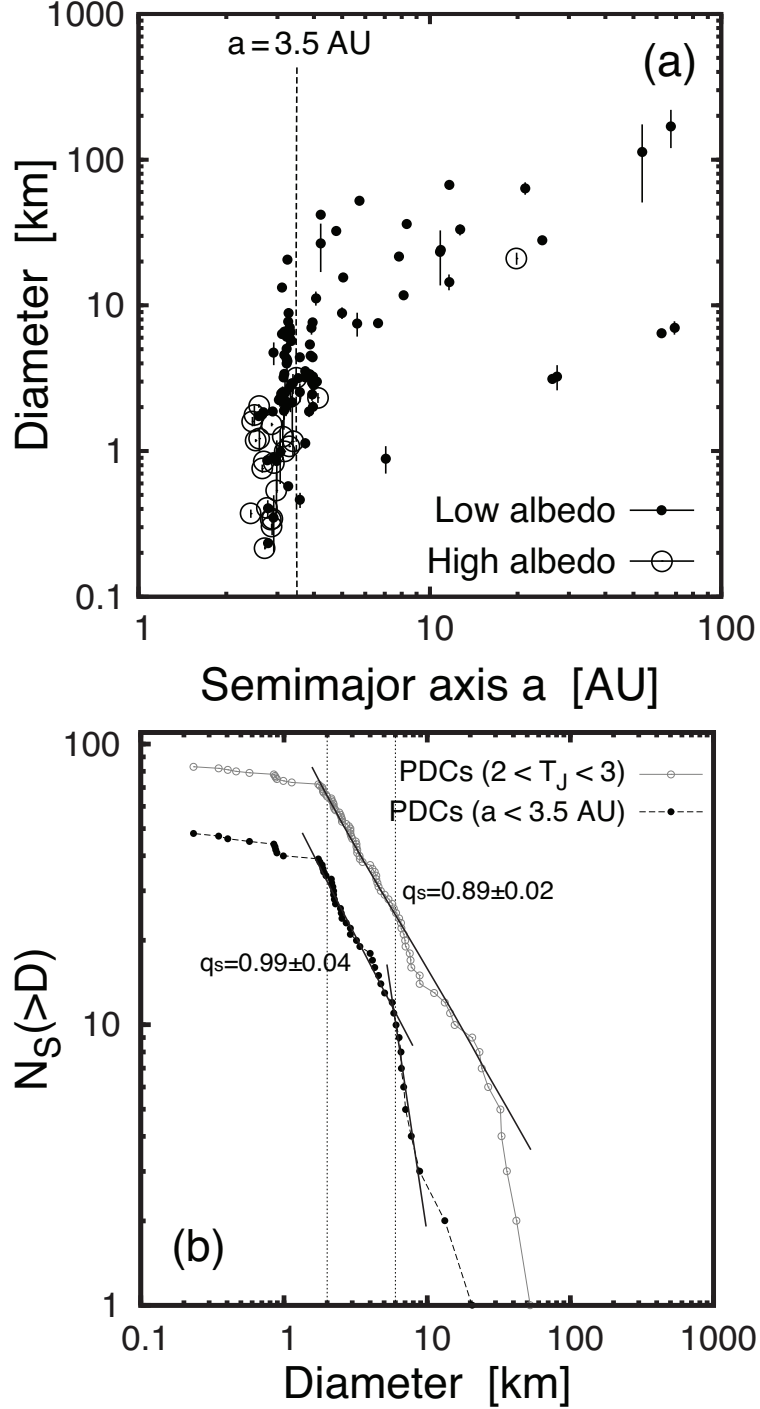


Fig. 7.— (a) Plot of the semimajor axis a vs. the diameter of asteroids in comet-like orbits. Open circles denote the high-albedo objects ($p_v \geq 0.1$); filled circles denote the low-albedo objects ($p_v < 0.1$). Small ($\lesssim 3$ km) objects were detected within $\lesssim 3.5$ AU. (b) Cumulative size distribution of PDCs. Open circles stand for all PDCs; filled circles stand for PDCs with $a < 3.5$ AU.

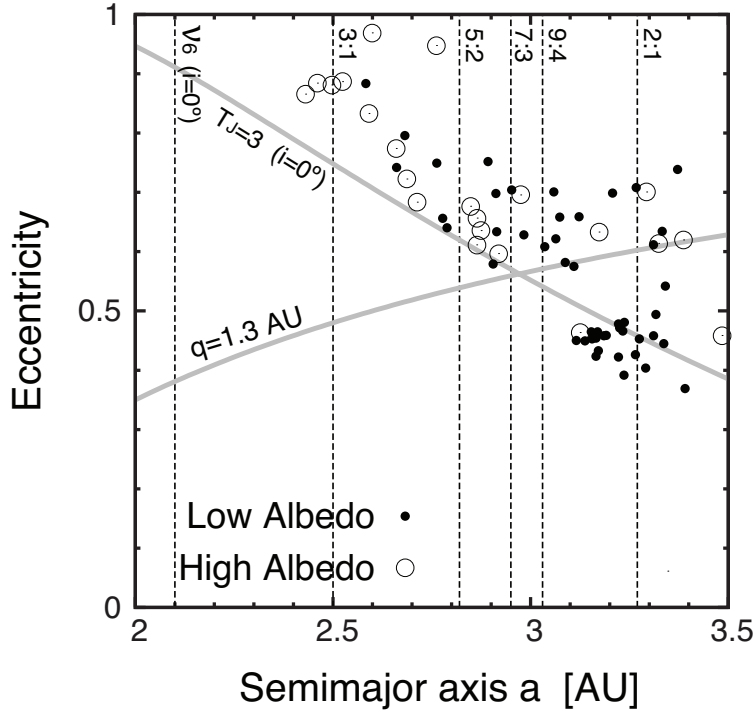


Fig. 8.— (a) Plot of the semimajor axis a vs. the eccentricity e of asteroids in comet-like orbits. Open circles denote the high-albedo objects ($p_v \geq 0.1$); filled circles denote the low-albedo objects ($p_v < 0.1$). A line of $q=1.3$ AU and $T_J = 3.0$ ($i=0^\circ$ is assumed) are drawn to clarify near-Earth objects and JFC-like objects. Vertical lines correspond to major resonances with planets.

Table 1: Astroids in Comet-like Orbits in Infrared Asteroidal Survey Catalogs

Number	Name	Desig	a [AU]	e	i [deg]	T_J	D [km]	p_v	Source
944	Hidalgo	1920 HZ	5.737	0.662	42.54	2.067	52.450 ± 3.600	0.042 ± 0.007	<i>AKARI</i>
1922	Zulu	1949 HC	3.237	0.481	35.42	2.734	20.561 ± 0.321	0.055 ± 0.006	<i>WISE</i>
3688	Navajo	1981 FD	3.222	0.478	2.56	2.996	6.086 ± 0.051	0.047 ± 0.012	<i>WISE</i>
3552	Don Quixote	1983 SA	4.222	0.713	30.96	2.316	26.656 ± 9.734	0.016 ± 0.009	<i>WISE</i>
5370	Taranis	1986 RA	3.333	0.634	19.09	2.731	5.821 ± 0.300	0.044 ± 0.009	<i>WISE</i>

Note. — This table is available in its entirety in a machine-readable form in the online journal. A portion is shown here for guidance regarding its form and content.